CAMBRIDGE
UNIVERSITY PRESS

Article

Optimization of ultrasonic-assisted copper ion removal from polluted water by a natural clinoptilolite nanostructure through a central composite design

Mohsen Sheydaei* iD, Ali Balanejad Gasemsoltanlu and Asadollah Beiraghi

Faculty of Chemistry, Kharazmi University, 15719-14911 Tehran, Iran

Abstract

A natural clinoptilolite nanostructure (CNS) along with ultrasonic irradiation was used to remove Cu^{2+} ions from polluted water. In the first part of this work, natural clinoptilolite was converted to CNS by ball milling. The natural clinoptilolite and prepared CNS samples were characterized by scanning electron microscopy (SEM), energy-dispersive X-ray spectroscopy, Fourier-transform infrared (FTIR) spectroscopy, X-ray diffraction, N_2 adsorption/desorption and pH at the point of zero charge analyses. The SEM images showed the development of CNS from natural clinoptilolite by ball milling. The N_2 adsorption/desorption and FTIR spectroscopy confirmed the greater specific surface area, pore volume and number of surface groups of the CNS compared to the natural clinoptilolite. In addition, the crystalline phase of the CNS was the same as the natural clinoptilolite. In the second part of this work, the ultrasonic-assisted sorption of Cu^{2+} ions from polluted water by CNS was investigated. These experiments were optimized with response surface methodology based on central composite designs. The effects of initial pH of solution, CNS dosage, sonication time and temperature on Cu^{2+} ion-removal efficiency were investigated. By using a CNS dosage of 500 mg L^{-1}, an initial pH of 6, a sonication time of 12 min and a sonication temperature of 45°C as optimal conditions, 97% of Cu^{2+} ions were removed from contaminated water. The initial pH was the most effective variable. Ultrasonic-assisted sorption of Cu^{2+} was more effective than sorption alone, onto the CNS.

The contamination of water resources by toxic chemicals, especially heavy metals, is a serious problem. The main sources of these non-degradable metal ions are industrial activities such as mining, ore processing and metal plating (Sanchez *et al.*, 1999; Entezari & Soltani, 2008). Among heavy metals, copper has special industrial significance due to its extensive use (Aber *et al.*, 2013). Therefore, it is important to remove copper ions from wastewaters before they are discharged into water resources. Numerous methods have been studied to remove copper ions from polluted waters. Sorption is regarded as a promising technology due to its advantages of easy operation, low cost and convenience (Stojakovic *et al.*, 2011). In recent years, many studies have been carried out on the ability to adsorb Cu^{2+} ions of natural sorbents such as palygorskite and vermiculite (Bourliva *et al.*, 2018), montmorillonite and palygorskite (Lin *et al.*, 2017), biomass ash (Xu *et al.*, 2018), volcanic tuff (Radaideh *et al.*, 2017), flax fibres (Abbar *et al.*, 2017), natural zeolite (Katsimicha *et al.*, 2017), natural sepiolite (Dönmez *et al.*, 2015) and kaolin and zeolitic tuff (Al-Makhadmeh & Batiha, 2016). Improving the sorption

rates and capacities of natural sorbents has become one of the main topics of current research. It has been established that the reduction of the particle size of natural sorbents to nano-dimensions leads to a greater number of available active sites, shorter diffusion path lengths and lower mass transfer resistance between the solution phase and the sorbent surface (Pourtaheri & Nezamzadeh-Ejhieh, 2015). Furthermore, ultrasonic waves may improve the rate and efficiency of the sorption process. Ultrasonic waves lead to an alternating adiabatic compression and rarefaction cycle of the liquid media that decreases the thickness of the liquid film attached to the solid phase and mass transfer resistances (Entezari & Soltani, 2008; Pang & Abdullah, 2013).

The classical 'one-factor-at-a-time' method has been used commonly to investigate and optimize the effects of various significant independent variables on the process. This method involves changing one variable at a time while making all other variables constant to study the effect of the variable on the response (Wu *et al.*, 2012). The one-factor-at-a-time method is time consuming and fails to consider any possible interactions between the independent variables in a multivariable system (Adamczyk *et al.*, 2008). These problems might be overcome by using experimental design methodologies. Among them, response surface methodology (RSM) is the most economical and convenient method utilized in many fields. The main idea behind RSM is

using statistical and mathematical techniques to develop and optimize processes (Song *et al.*, 2011).

The main objectives of this work were to reduce the size of natural clinoptilolite particles to the nanoscale and to use them in ultrasonic-assisted sorption of Cu^{2+} ions from contaminated solution, as well as to investigate the effect of clinoptilolite nanostructure (CNS) dosage, pH, sonication time and temperature as independent variables on ultrasonic-assisted sorption and to optimize the process.

Materials and methods

Materials

Natural clinoptilolite with an average grain size of 125 μm were obtained from Afarazand Co., Iran. Copper nitrate thrihydrate $(Cu(NO_3)_2 \cdot 3H_2O)$, nitric acid (HNO_3), sodium nitrate $(NaNO_3)$ and sodium hydroxide (NaOH) were obtained from Merck. Distilled water was used throughout the study.

Preparation of CNS

The natural clinoptilolite was treated by mechanical ball milling to prepare the appropriate nanostructure. Accordingly, the natural clinoptilolite powder with a size distribution of <125 μm was milled in a high-energy planetary ball mill (MLP, Sanat Eeram Mehr Alborz, Iran) at a rotational speed of 600 rpm. The ratio of the bullet weight to the clinoptilolite powder weight was 4 and the grinding time was 6 h. The CNS obtained was washed with distilled water and dried in a vacuum oven at 80°C.

Characterization techniques

The morphology and the size of the sample particles were analysed using a ZEISS EVO-18 scanning electron microscope (SEM). The IR spectra of the particles were collected with a Perkin Elmer Fourier-transform infrared spectrometer using the KBr disc method. The specific surface areas and total pore volumes of the natural clinoptilolite and CNS samples were estimated using the Brunauer–Emmett–Teller (BET) method with a Belsorp-Mini surface analyser (Japan) by N_2 adsorption/desorption at 77 K. The sample phases were identified by X-ray diffraction (XRD; Philips X'Pert).

The pH at the point of zero charge (pH_{pzc}) of the natural clinoptilolite and the CNS samples was determined according to the salt addition method. Accordingly, a series of 40 mL 0.01 M $NaNO_3$ solutions were prepared and transferred to Erlenmeyer flasks. The pH values of the solutions were adjusted from 1 to 10 by adding dilute HNO_3 or NaOH solutions. Approximately 0.6 g of sample was added to each solution, and the suspensions obtained were stirred for 72 h. The final pH of each solution was measured. The differences between the initial and final pH values (ΔpH) were plotted against the related initial pH values (pH_i). The pH_{pzc} was the pH at which ΔpH was equal to zero.

Batch ultrasonic-assisted sorption experiments

Ultrasonic-assisted sorption experiments were conducted in a 100 mL glass reactor. Ultrasonication of the glass reactor was carried out in an ultrasonic bath (Parsonic 7500s, Pars Nahand Engineering Co., Iran) at a frequency of 28 kHz and a power of 100 W. A total of 50 mL of 10 mg L^{-1} Cu^{2+} solutions was used during the ultrasonic-assisted sorption processes. A predetermined amount of the CNS was added to the reactor and mixed with the Cu^{2+} solution. The pH of the suspension was adjusted from 2 to 6 by addition of NaOH and HNO_3. The experiments were performed at various temperatures. After conducting the experiments and before carrying out the analyses, the samples were filtered using a 0.22 μm membrane to separate the CNS. A Varian SpecterAA-20 Atomic Absorption Spectrometer (Palo Alto, CA, USA) equipped with a Cu hollow cathode lamp was used for the determination of Cu^{2+} concentration.

Experimental design

For the experimental setup design, a central composite design (CCD) matrix of the RSM was applied to investigate the effect of CNS dosage (x_1, g L^{-1}), pH (x_2), sonication time (x_3, min) and sonication temperature (x_4, °C), as independent variables, on the removal efficiency of Cu^{2+} (10 mg L^{-1}), as the dependent variable, using *Design Expert 8.0* software. The four independent variables and their levels in coded and actual values are listed in Table 1. Furthermore, the total number of 31 experimental runs with six centre points are shown in Table 2. In developing the regression equation, the relationship between the coded values and the actual values is described by equation 1:

$$X_i = \frac{(x_i - x_0)}{\Delta x} \qquad (1)$$

where X_i is a coded value of the independent variable, x_i is the actual value of the independent variable, x_0 is the actual value of the independent variable at the centre point level and Δx is the step change value between the centre point level and high level (+1).

The Cu^{2+} removal efficiency data from CCD-proposed experimental runs were analysed by multiple regressions to fit the following second-order polynomial model (equation 2):

$$Y = \beta_0 + \sum_{i=1}^{k} \beta_i X_i + \sum_{i=1}^{k} \beta_{ii} X_i^2 + \sum_{i=1}^{k-1} \sum_{j=2}^{k} \beta_{ij} X_i X_j + \varepsilon \qquad (2)$$

where Y is the Cu^{2+} removal efficiency as the dependent variable; β_0, β_i, β_{ii} and β_{ij} are the constant, linear, squared and interaction coefficients of the model, respectively; X_i, X_i^2 and $X_i X_j$ are the linear, quadratic and interaction terms of model, respectively; i/j must be considered in the interaction term ($X_i X_j$); k is the number of factors studied and ε is the error. Statistical analysis was used to evaluate the fit quality of the experimental results to the polynomial model.

Sorption isotherm

The sorption isotherm was obtained at room temperature and a pH of 6. A total of 30 mg of sorbent was placed in a conical flask containing 50 mL of Cu^{2+} aqueous solutions of initial concentrations varying from 50 to 500 mg L^{-1}. After sorption for 2 days, the equilibrium concentrations of Cu^{2+} in the solutions were determined. The concentrations sorbed were calculated

Table 1. Actual and coded levels of the variables used for the ultrasonic-assisted sorption process by CCD.

	Variable level				
Independent variable	−2	−1	0	+1	+2
CNS dosage (x_1, g L^{-1})	100	200	300	400	500
pH (x_2)	2	3	4	5	6
Time (x_3, min)	0	3	6	9	12
Temperature (x_4, °C)	5	15	25	35	45

Table 2. Experimental design and the results of the CCD.

Experiment order	x_1 (g L^{-1})	x_2	x_3 (min)	x_4 (°C)	Y (%, experimental)
1	300	4	0	25	0
2	400	3	9	15	32
3	300	4	6	45	90
4	300	4	6	25	69
5	400	3	3	35	38
6	200	3	3	15	34
7	400	5	9	15	90
8	400	5	3	15	51
9	400	3	9	35	50
10	300	4	6	5	40
11	300	4	6	25	52
12	300	4	6	25	46
13	200	5	3	15	76
14	400	5	9	35	70
15	400	3	3	15	30
16	400	5	3	35	80
17	300	2	6	25	28
18	200	5	9	15	67
19	300	4	6	25	60
20	300	6	6	25	81
21	200	3	3	35	34
22	200	5	3	35	57
23	300	4	6	25	46
24	300	4	6	25	46
25	200	3	9	15	25
26	500	4	6	25	88
27	200	5	9	35	56
28	200	3	9	35	36
29	300	4	12	25	56
30	100	4	6	25	30

according to equation 3 (Sheydaei & Aber, 2013):

$$q_e = (C_0 - C_e)V/M \qquad (3)$$

where q_e (mg g^{-1}) is the amount of Cu^{2+} sorbed on the mass of the sorbent, C_0 (mg L^{-1}) is the initial Cu^{2+} solution concentration and C_e (mg L^{-1}) is the equilibrium Cu^{2+} solution concentration. M and V are the weight of the sorbent (g) and volume of the solution (L), respectively.

In addition, two isotherm equations (Freundlich and Langmuir) were adopted in this work to study the sorption capacities of the natural clinoptilolite and CNS. The Freundlich isotherm is represented by equation 4 (Wang *et al.*, 2015):

$$\log q_e = \log K_f + (1/n)\log C_e \qquad (4)$$

where $1/n$ is the slope showing the variation of the sorption with concentration and K_f is the intercept showing the sorption capacity of the sorbent.

The Langmuir equation is expressed by equation 5 (Mustafai *et al.*, 2018):

$$C_e/q_e = C_e/Q_{max} + 1/bQ_{max} \qquad (5)$$

where Q_{max} (mg g^{-1}) and b (L mg^{-1}) are constants related to the sorption capacity and energy of sorption, respectively.

Results and discussion

Characterization of the CNS

The SEM images of the natural clinoptilolite and CNS samples are shown in Fig. 1a,b. Comparison of the SEM images of the clinoptilolite particles before and after ball milling showed the development of nanometre-sized particles due to the mechanical process. *Manual Microstructure The Distance Measurement* software (version 2.0, Nahamin Pardazan Asia Co., Iran) was used to determine the size distribution of the clinoptilolite treated by ball milling. The mode of the CNS particle size was 80–90 nm (Fig. 1c), suggesting the nanostructured nature of the clinoptilolite. Figure 1d shows the energy-dispersive X-ray spectra of the nanostructure produced. The elemental composition (wt.%) was O (46.37), Na (2.65), Al (6.64), Si (39.30) and K (5.05).

The N_2 adsorption/desorption isotherm was used to characterize the pore structure of the natural clinoptilolite and CNS. Based on the International Union of Pure and Applied Chemistry (IUPAC) classification, the adsorption/desorption isotherm for both samples is of type IV, along with a hysteresis loop at high partial pressure associated with capillary condensation, which indicates the existence of mesoporous structures in the natural clinoptilolite and CNS (Fig. 2).

The total pore volumes of the natural clinoptilolite and the CNS were 0.06 and 0.1 cm^3 g^{-1}, respectively. According to the Barrett–Joyner–Halenda (BJH) method, the mesoporous surface area and pore volume were 9.00 cm^2 g^{-1} and 0.06 cm^3 g^{-1}, respectively, for the natural clinoptilolite and 17.12 m^2 g^{-1} and 0.11 cm^3 g^{-1}, respectively, for the CNS. A comparison of the pore volume of the CNS with that of natural clinoptilolite indicates that the porosity of the natural silicate increased due to the development of the nanostructure. The pores developed are mainly in the mesoporous range (2–50 nm).

The XRD traces (Fig. 3) of the natural clinoptilolite and CNS samples indicate the existence of diffraction peaks at 10, 11.4, 17.4, 23, 26, 28.2, 30.2, and 32°2θ, typical of clinoptilolite. By comparing the XRD traces of both samples, no significant shifts were seen in the peak positions of the natural clinoptilolite and CNS samples. However, the XRD trace of the CNS sample displays a hump in the 20–30°2θ range, suggesting amorphization of the clinoptinolite during ball milling. Moreover, the intensity of CNS XRD peaks was lower than that of natural clinoptilolite peaks, which may be attributed to the decrease in the crystal order of the zeolite. Similar results were reported for the preparation of martite nanocatalyst from natural martite by high-energy planetary ball milling (Dindarsafa *et al.*, 2017).

The FTIR spectra obtained from both the natural clinoptilolite and CNS samples in the range of 400–4000 cm^{-1} are shown in Fig. 4. In the spectrum for natural clinoptilolite, a broad band was observed between 980 and 1200 cm^{-1} corresponding to the Si–O–Si asymmetric and Si–OH symmetric stretching vibrations (Sun *et al.*, 2014). The absorption band at 784 cm^{-1} belongs to the Al–O stretching vibration (Khataee *et al.*, 2016). The bands
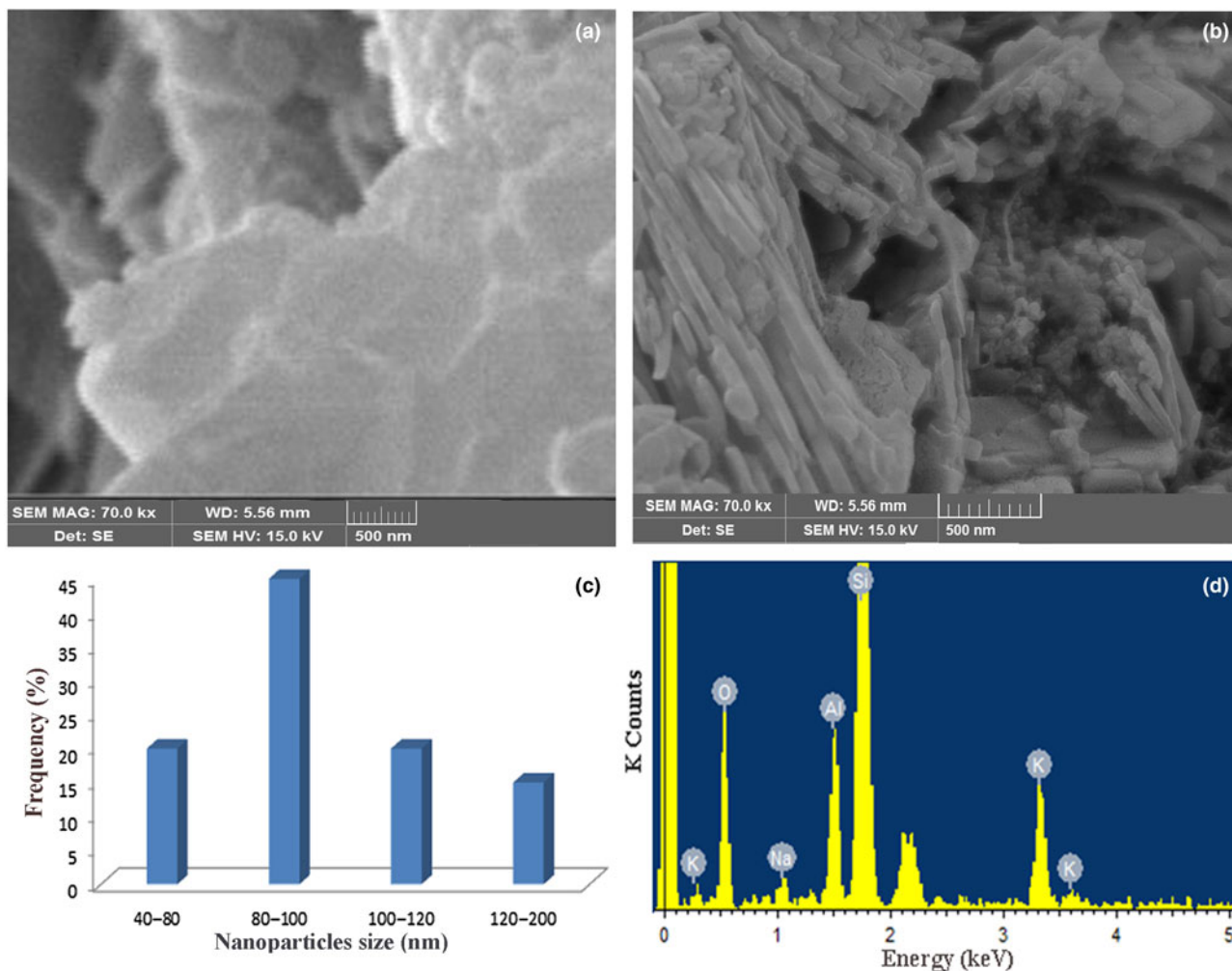
Fig. 1. SEM images of (a) the natural clinoptilolite particles and (b) CNS, (c) size distribution and (d) energy-dispersive X-ray spectra of the CNS produced.
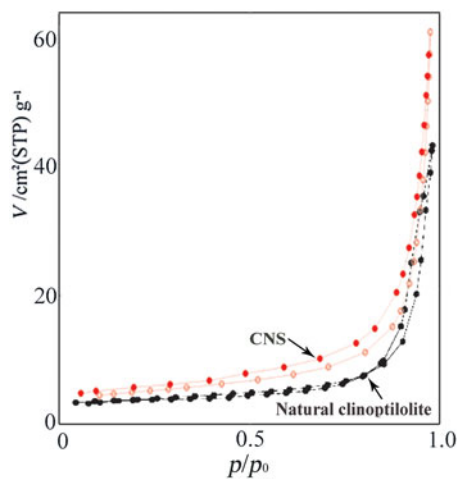
Fig. 2. N$_2$ adsorption/desorption isotherms of the natural clinoptilolite and CNS samples. STP = standard temperature and pressure.
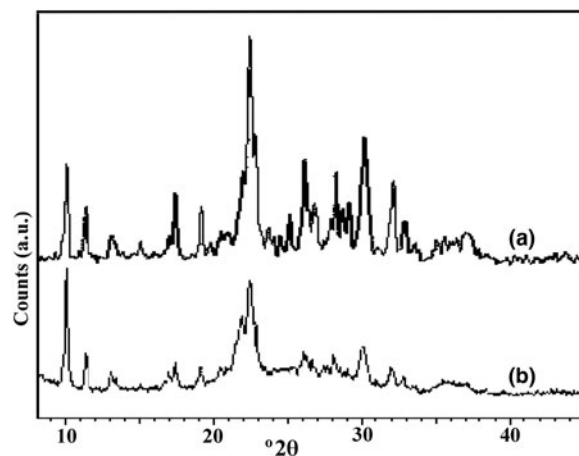
Fig. 3. XRD traces of the (a) natural clinoptilolite and (b) CNS samples.

at 3617, 3448 and 1634 cm^{-1} are due to the –OH stretching vibration, adsorbed H$_2$O deformation and H–OH bending vibration, respectively (Zhang *et al.*, 2010). Similar absorption bands observed for the CNS sample indicate that the ball milling did not affect

significantly the structure of the natural clinoptilolite. Furthermore, the observed frequencies for both samples are in good agreement with published FTIR data on clinoptilolite (Pourtaheri & Nezamzadeh-Ejhieh, 2015). Meanwhile, the
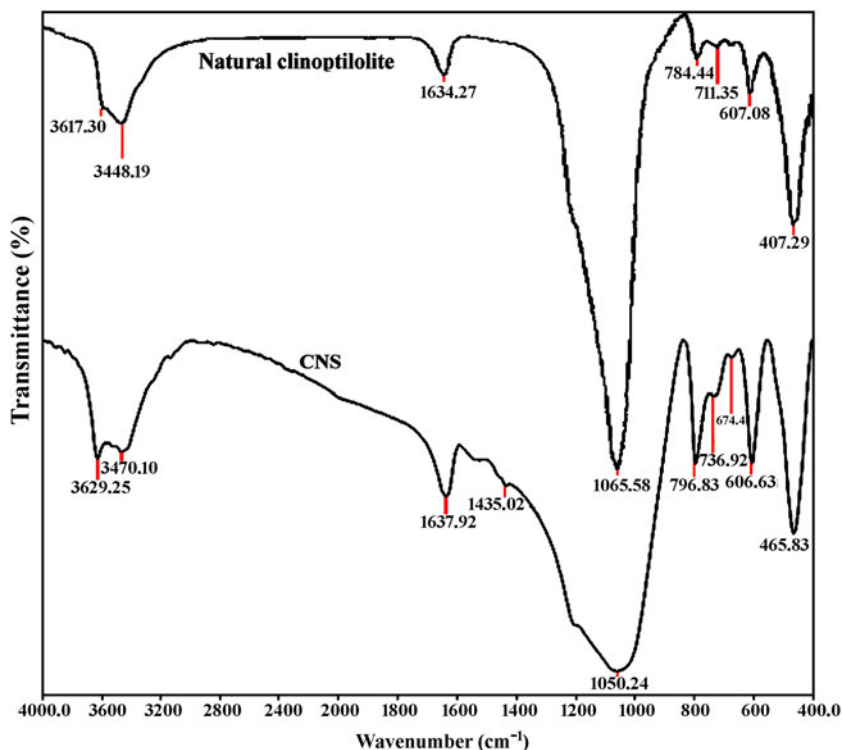
Fig. 4. FTIR spectra of the natural clinoptilolite and CNS samples.
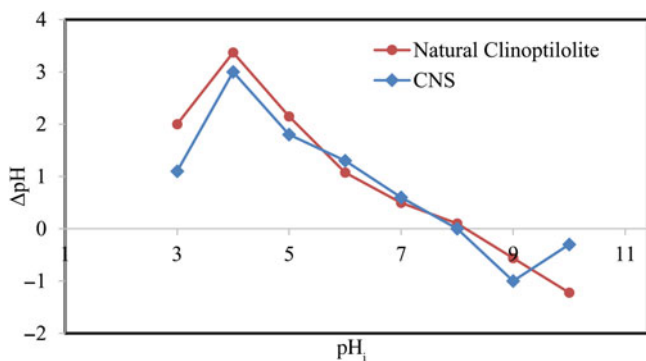
Fig. 5. ΔpH vs pH$_i$ plots for the determination of pH$_{pzc}$ of the natural clinoptilolite and CNS samples.

Table 3. ANOVA for the response surface quadratic model.

Source	Degrees of freedom	F-value	p-value
Model	19	9.09	0.0005
x_1	1	21.83	0.0009
x_2	1	75.65	<0.0001
x_3	1	20.35	0.0011
x_4	1	16.22	0.0024
$x_1 \times x_2$	1	0.159	0.6985
$x_1 \times x_3$	1	2.92	0.1183
$x_1 \times x_4$	1	2.37	0.1551
$x_2 \times x_3$	1	0.12	0.7396
$x_2 \times x_4$	1	2.73	0.1295
$x_3 \times x_4$	1	0.32	0.5815
x_1^2	1	0.76	0.4046
x_2^2	1	0.04	0.8463
x_3^2	1	14.09	0.0038
x_4^2	1	3.12	0.1080
$x_1 \times x_3 \times x_4$	1	2.73	0.1295
$x_2 \times x_3 \times x_4$	1	3.12	0.1079
$x_1^2 \times x_3$	1	10.61	0.0086
$x_1^2 \times x_4$	1	9.16	0.0128
$x_1 \times x_2^2$	1	8.38	0.0160
Residual	10		
Lack of fit	5	0.70	0.6467
Pure error	5		
Total	29		

intensities of some of the IR bands related to the CNS sample, especially the band at 796 cm^{-1} corresponding to amorphous SiO$_2$ formed during milling, indicate that the ball milling resulted in larger surface groups and bands due to increases in the specific surface area.

Figure 5 shows the initial pH value (pH$_i$) plotted against the difference between the initial and final pH values (ΔpH) of the suspensions to determine the pH$_{pzc}$ of the natural clinoptilolite and CNS samples. pH values of 8.0 and 8.3 are considered to be the pH$_{pzc}$ values of the natural clinoptilolite and CNS samples, respectively. At pH$_{pzc}$, the surface has net electrical neutrality with amphoteric properties, which act as a buffer. The surfaces of the particles are positive at pH values lower than the pH$_{pzc}$ and negative at pH values higher than the pH$_{pzc}$. The surface charge density of the material should decrease when the pH of the solution approaches the pH$_{pzc}$ and increase as it deviates from the pH$_{pzc}$. Comparison

of the pH$_{pzc}$ values of the natural clinoptilolite and CNS samples shows that the surface structure of the natural clinoptilolite remained unchanged during high-energy planetary ball milling.

Model development and analysis

The results regarding copper removal for all of the experiments designed using the CCD method (Table 2) were analysed using *Design-Expert* 7.0.0 software and the following mathematical
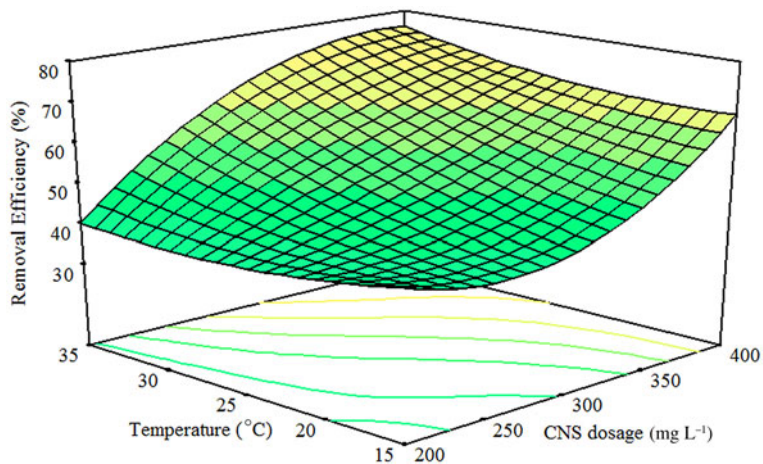
Fig. 6. Effect of sonication temperature and CNS dosage on the removal efficiency of copper ions (experimental conditions: pH = 4, [Cu^{2+}]$_0$ = 10 mg L^{-1}, sonication time = 6 min).
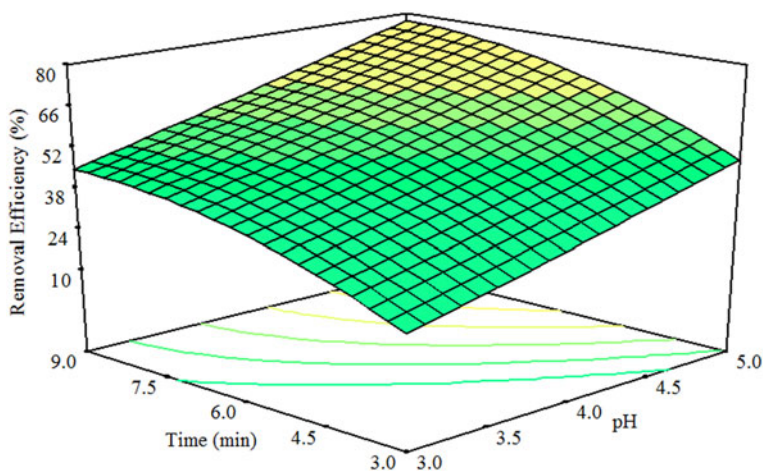
Fig. 7. Effect of initial pH and sonication time on the removal efficiency of copper ions (experimental conditions: [Cu^{2+}]$_0$ = 10 mg L^{-1}, sonication temperature = 25°C).

model of the ultrasonic-assisted sorption process was introduced:

$$Cu^{2+} \text{removal (\%)} = 53.17 + 14.50 \times X_1 + 15.58 \times X_2$$
$$+ 14.00 \times X_3 + 12.50 \times X_4 + 0.87 \times X_1 \times X_2$$
$$+ 3.75 \times X_1 \times X_3 + 3.37 \times X_1 \times X_4$$
$$+ 0.75 \times X_2 \times X_3 - 3.63 \times X_2 \times X_4$$
$$- 1.25 \times X_3 \times X_4 + 1.46 \times X_1^2 + 0.33 \times X_2^2 - 6.29 \times X_3^2$$
$$+ 2.96 \times X_4^2 - 3.62 \times X_1 \times X_3 \times X_4 - 3.88 \times X_2 \times X_3 \times X_4$$
$$- 12.38 \times X_1^2 \times X_3 - 11.50 \times X_1^2 \times X_4 - 11.00 \times X_1 \times X_2^2$$
$$\tag{6}$$

In this model, the negative-signed terms have an antagonistic effect and the positive-signed terms have a synergistic effect on ultrasonic-assisted removal of copper ions from water.

An analysis of variance (ANOVA) test was performed to justify the adequacy of the mathematical model developed. The first index is the p-value of the Fisher F test (prob. > F). The prob. > F for the proposed model was 0.0005 (Table 3), which indicates that the model is significant. Furthermore, the lack of fit (LOF) prob. > F value of 0.6467 implies that LOF is not significant. The significant model and nonsignificant LOF values indicate the suitability of the proposed model for Cu^{2+} ultrasonic-assisted removal by the CNS.

After a statistical justification and assurance of the adequacy of the model developed, all of the terms within the model were also analysed statistically with the F-test to determine their importance in the model. The results for F-values and their p-values are shown in Table 3. By examining the significance tests of each of the independent effective factors and interactions among all the terms of the model with a change in levels, the effects of x_1, x_2, x_3, x_4, x_3^2, $x_1^2 \times x_3$, $x_1^2 \times x^4$ and $x^1 \times x_2^2$ on Cu^{2+} removal efficiency are significant.

Response surface and contour plots for Cu^{2+} removal

The effects of CNS dosage at various sonication temperatures on the removal efficiency of copper ions at pH 4 and a sonication time of 6 min are shown in Fig. 6. The removal efficiency increases with increase of the CNS dosage and sonication temperature. The increase in the removal efficiency may be attributed to the increase in the number of active sorption sites resulting from increase in the sorbent dosage. A similar result was also reported in studies on the sorption of chemical pollutants by natural sorbents (Wang *et al.*, 2011; Bourliva *et al.*, 2013).

At low CNS dosages, the sonication temperature does not have a significant effect on the sorption efficiency (Fig. 6). However, in the presence of greater doses of sorbent, the sorption efficiency increases with temperature. The effects of temperature on
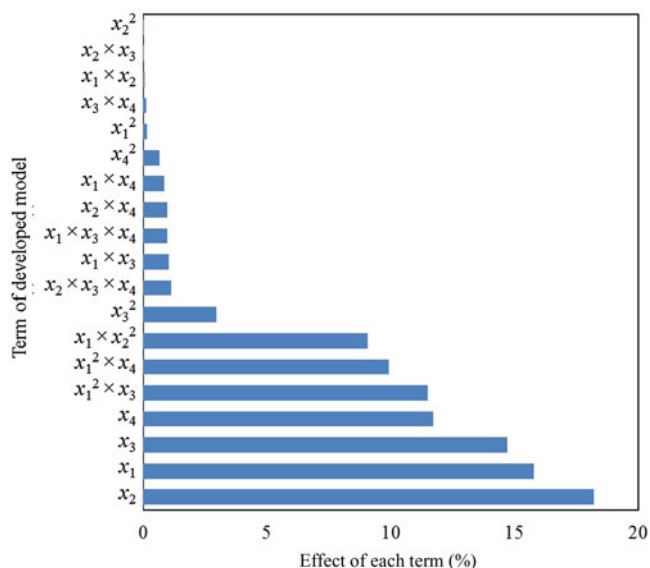
Fig. 8. Percentage effect of each model term obtained using Pareto analysis.

enhancing the mass transfer and pore diffusion rates of pollutants are considered to be the main reasons for the increase in the removal efficiency with sonication temperature. This leads to an increase in number of effective contacts between sorbate and sorbent. On the other hand, the increase in sonication temperature may affect the size of the clinoptilolite pore structure, which may also lead to an increase in the removal efficiency of copper ions. Moreover, it can be inferred that the sorption of copper ions by clinoptilolite is an endothermic process that occurs via physical sorption. Similar results have been reported for the surface uptake of Cu^{2+} ions on almond shells (Aber *et al.*, 2011).

The effects of the initial pH of the solution and sonication time on the Cu^{2+} removal efficiency at 25°C are shown in Fig. 7. The Cu^{2+} removal efficiency increases with increasing initial pH due to the reduction in the H^+ concentration. The Cu^{2+} ions compete strongly with H^+ ions for sorption on the clinoptilolite surface at low pH values, whereas with increasing pH values, the Cu^{2+} loading onto the sorbent surface increases. A similar result has been reported for modified montmorillonite absorbing Pb and Cu (Sani *et al.*, 2017). In addition, the removal efficiency of Cu^{2+} increased slightly with sonication time (Fig. 7). This might be

attributed to an increase in the mass transfer of Cu^{2+} ions from the solution to the surface of CNS.

Optimization results

An optimization study was performed to determine the optimal levels of the experimental variables for maximization of the ultrasonic-assisted removal efficiency of Cu^{2+} ions and to assess the performance of the process under these conditions. Based on the regression model (equation 6) and ANOVA results, the optimum values of the CNS dosage, initial pH, sonication time and temperature for the maximum Cu^{2+} removal efficiency were 500 mg L^{-1}, 6, 12 min and 45°C, respectively. Under these conditions, the predicted Cu^{2+} removal rate was 100%, while the experimental removal rate was ~97%. Thus, equation 6 may be used as a mathematical model of ultrasonic-assisted removal.

Pareto analysis

To obtain the percentage effect of each term of the developed model on the Cu^{2+} removal efficiency, Pareto analysis was performed using equation 7:

$$p_i = \left(\frac{X_i^2}{\sum X_i^2} \right) \times 100 (i \neq 0) \qquad (7)$$

Figure 8 shows the Pareto graphic analysis. The initial pH produces the greatest effect on ultrasonic-assisted removal efficiency (18.23%) among the variables tested.

Comparison experiments

The comparison of sorption and ultrasonic-assisted sorption of Cu^{2+} from polluted water by CNS with sorption of this pollutant by natural clinoptilolite microstructures and precipitation (sorbent-free) processes is presented in Fig. 9 (experimental conditions were initial Cu^{2+} concentration of 10 mg L^{-1} at an initial pH of 6 with a sonication time of 12 min and a sonication temperature of 45°C). The Cu^{2+} ions did not precipitate at pH 6 (Fig. 9). In addition, the decrease in size of clinoptilolite particles enhanced the ability of this natural zeolite for sorption of Cu^{2+} from polluted water. Furthermore, ultrasonic irradiation may improve the Cu^{2+} removal efficiency by CNS due to increase of the contaminant mass-transfer rate around the liquid–solid
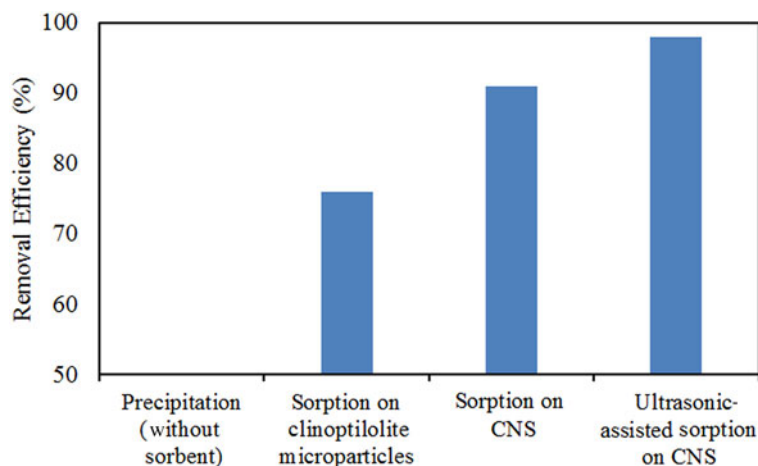
Fig. 9. Comparison of Cu^{2+} removal (%) by precipitation and sorption on natural clinoptilolite microstructures and CNS with ultrasonic-assisted sorption of Cu^{2+} using CNS (experimental conditions: sorbent dosage = 500 mg L^{-1}, $[Cu^{2+}]_0 = 10$ mg L^{-1}, initial pH = 6, sonication time = 12 min, sonication temperature = 45°C).
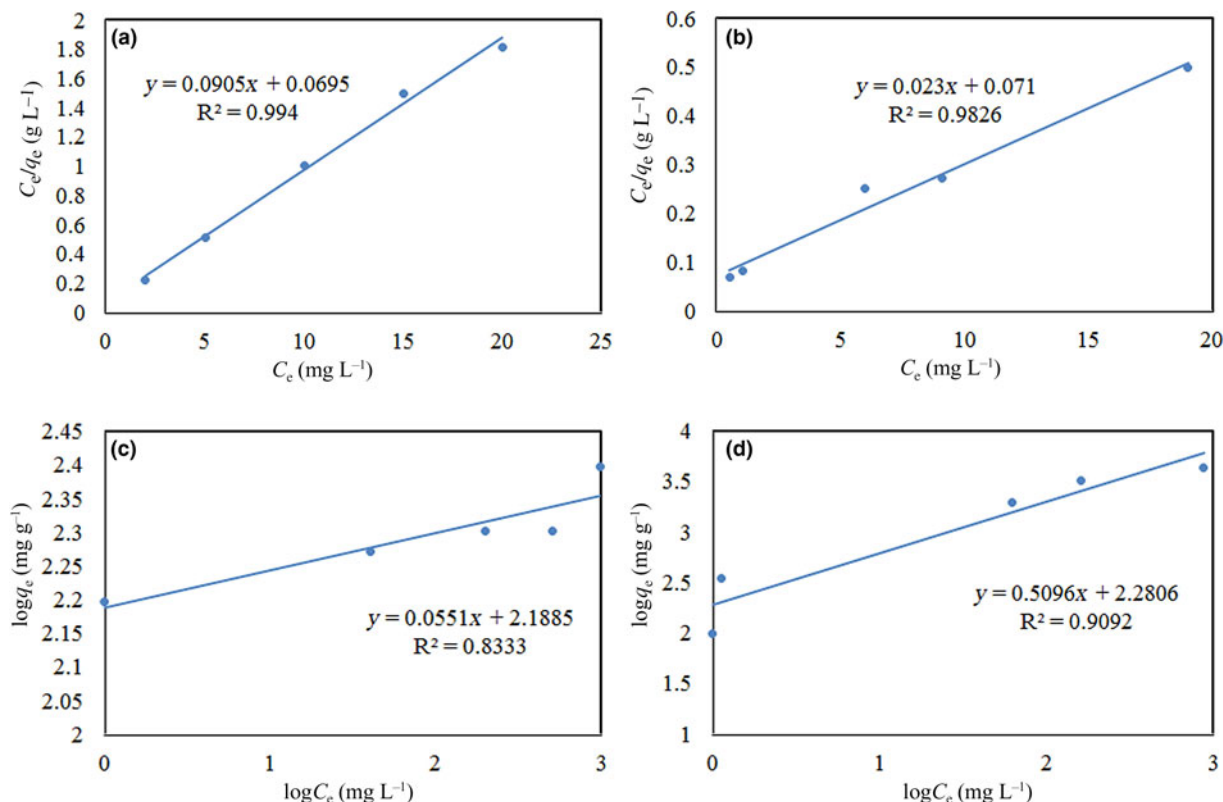
Fig. 10. Langmuir isotherms for Cu^{2+} sorption onto (a) natural clinoptilolite and (b) CNS and Freundlich isotherms for Cu^{2+} sorption onto (c) natural clinoptilolite and (d) CNS.

Table 4. Langmuir and Freundlich parameters for sorption of Cu^{2+} on the natural clinoptilolite and CNS samples.

Isotherm model	Parameter	Natural clinoptilolite	CNS
Langmuir	b (L mg^{-1})	1.30	0.32
	Q_{max} (mg g^{-1})	11.05	43.48
	R^2	0.99	0.98
Freundlich	K_f (mg g^{-1})(mg L^{-1})^n	154.17	190.55
	n	18.15	1.96
	R^2	0.83	0.91

Table 5. Reported equilibrium sorption capacity for Cu^{2+} on natural clinoptilolite samples in comparison with CNS samples.

Sorbent	Equilibrium sorption capacity (mg g^{-1})	Reference
CNS	43.48	This work
Natural clinoptilolite (China)	26.80	Wang & Huang (2010)
Natural clinoptilolite (Ukraine)	25.69	Sprynskyy *et al.* (2006)
Natural clinoptilolite (Iran)	13.09	Irannajad *et al.* (2016)

interface via acoustic waves, microscopic turbulence and the high localized temperature during the collapse of cavitation bubbles.

Sorption isotherm

The q_e and C_e values obtained from the sorption isotherm experiments were fitted to the Langmuir model by plotting C_e/q_e *vs* C_e (Fig. 10a,b). Furthermore, Fig. 10c,d illustrates a plot of $\log q_e$ *vs* $\log C_e$ to fit the experimental data with the Freundlich isotherm.

Isotherm parameters for the models and correlation coefficients (R^2) were calculated and are listed in Table 4. Both the Langmuir and the Freundlich isotherms generated satisfactory fits to the experimental data with consideration of the correlation coefficients. However, the Langmuir isotherm shows a better fit to the sorption data of both natural clinoptilolite and CNS samples than the Freundlich isotherm (Table 4). According to the Langmuir equation assumptions, distribution of sorbate on the homogenous natural clinoptilolite and CNS surfaces is monolayer. Comparison of the values of the maximum sorption capacities for Cu^{2+} on the natural clinoptilolite (11.05 mg g^{-1}) and CNS (43.48 mg g^{-1}) indicates the increase in sorption capacity of clinoptilolite by the ball-milling process.

Comparison of CNS with other natural clinoptilolite samples

A comparison of the sorption capacity for Cu^{2+} ions on the CNS with that of the other natural zeolite sorbents reported in previous works is shown in Table 5. The CNS shows a greater sorption capacity in comparison to natural clinoptilolite samples. Therefore, the ball-milling process may be suitable for increasing the sorption capacity of natural clinoptilolite.

Conclusions

The preparation of CNS from natural clinoptilolite and using ultrasound irradiation increases the efficiency of natural zeolite in terms of the removal of Cu^{2+} ions from the aqueous phase. The process was optimized by RSM based on CCD. Approximately 97% of the Cu^{2+} ions were removed under the

following optimized operational variables: a CNS dosage of 500 mg L^{-1}, an initial pH of 6, a sonication time of 12 min and a sonication temperature of 45ºC. The initial pH was the most important individual parameter. The efficiency of removal of Cu^{2+} via the ultrasonic-assisted sorption processes was greater than that achieved by sorption alone onto the CNS.

References

Abbar B., Alem A., Marcotte S., Pantet A., Ahfir N.-D., Bizet L. & Duriatti D. (2017) Experimental investigation on removal of heavy metals (Cu^{2+}, Pb^{2+}, and Zn^{2+}) from aqueous solution by flax fibres. *Process Safety and Environmental Protection*, **109**, 639–647.

Aber S., Ayoubi-Feiz B. & Salari D. (2013) Investigation of isothermal and fixed-bed column sorption of Cu(II) onto almond shell. *Environmental Engineering and Management Journal*, **12**, 435–441.

Aber S., Salari D. & Ayoubi Feiz B. (2011) The sorption of copper on almond shell: optimization and kinetics. *Water Science & Technology*, **63**, 1389–1395.

Adamczyk J., Horny N., Tricoteaux A., Jouan P.Y. & Zadam M. (2008) On the use of response surface methodology to predict and interpret the preferred c-axis orientation of sputtered AlN thin films. *Applied Surface Science*, **254**, 1744–1750.

Al-Makhadmeh L. & Batiha M.A. (2016) Removal of iron and copper from aqueous solutions using Jordanian kaolin and zeolitic tuff. *Desalination and Water Treatment*, **57**, 20930–20943.

Bourliva A., Michailidis K., Sikalidis C., Filippidis A. & Betsiou M. (2013) Lead removal from aqueous solutions by natural Greek bentonites. *Clay Minerals*, **48**, 771–787.

Bourliva A., Sikalidis A.K., Papadopoulou L., Betsiou M., Michailidis K., Sikalidis C. & Filippidis A. (2018) Removal of Cu^{2+} and Ni^{2+} ions from aqueous solutions by adsorption onto natural palygorskite and vermiculite. *Clay Minerals*, **53**, 1–15.

Dindarsafa M., Khataee A., Kaymak B., Vahid B., Karimi A. & Rahmani A. (2017) Heterogeneous sono-Fenton-like process using martite nanocatalyst prepared by high energy planetary ball milling for treatment of a textile dye. *Ultrasonics Sonochemistry*, **34**, 389–399.

Dönmez M., Camcı S., Akbal F. & Yağan M. (2015) Adsorption of copper from aqueous solution onto natural sepiolite: equilibrium, kinetics, thermodynamics, and regeneration studies. *Desalination and Water Treatment*, **54**, 2868–2882.

Entezari M.H. & Soltani T. (2008) Simultaneous removal of copper and lead ions from a binary solution by sono-sorption process. *Journal of Hazardous Materials*, **160**, 88–93.

Irannajad M., Haghighi H.K. & Safarzadeh E. (2016) Kinetic, thermodynamic and equilibrium studies on the removal of copper ions from aqueous solutions by natural and modified clinoptilolites. *Korean Journal of Chemical Engineering*, **33**, 1629–1639.

Katsimicha D., Pentari D., Pantelaki O. & Komnitsas K. (2017) Effect of wet milling on the adsorption capacity of a Greek natural zeolite used for the removal of heavy metals from solutions. *Bulletin of the Geological Society of Greece*, **47**, 953–962.

Khataee A., Kiranşan M., Karaca S. & Arefi-Oskoui S. (2016) Preparation and characterization of NnO/MMT nanocomposite for photocatalytic ozonation of a disperse dye. *Turkish Journal of Chemistry*, **40**, 546–564.

Lin S., Zhou T. & Yin S. (2017) Properties of thermally treated granular montmorillonite–palygorskite adsorbent (GMPA) and use to remove Pb^{2+} and Cu^{2+} from aqueous solutions. *Clays and Clay Minerals*, **65**, 184–192.

Mustafai F.A., Balouch A., Abdullah, Jalbani N., Bhanger M.I., Jagirani M.S., Kumar A. & Tunio A. (2018) Microwave-assisted synthesis of imprinted polymer for selective removal of arsenic from drinking water by applying Taguchi statistical method. *European Polymer Journal*, **109**, 133–142.

Pang Y.L. & Abdullah A.Z. (2013) Fe^{3+} doped TiO$_2$ nanotubes for combined adsorption–sonocatalytic degradation of real textile wastewater. *Applied Catalysis B: Environmental*, **129**, 473–481.

Pourtaheri A. & Nezamzadeh-Ejhieh A. (2015) Photocatalytic properties of incorporated NiO onto clinoptilolite nano-particles in the photodegradation process of aqueous solution of cefixime pharmaceutical capsule. *Chemical Engineering Research and Design*, **104**, 835–843.

Radaideh J.A., Barjenbruch M., Patzer S. & Shatnawi Z. (2017) Heavy metals removal using natural Jordanian volcanic tuff. *GSTF Journal of Engineering Technology (JET)*, **2**, 1–8.

Sanchez A.G., Ayuso E.A. & De Blas O.J. (1999) Sorption of heavy metals from industrial waste water by low-cost mineral silicates. *Clay Minerals*, **34**, 469–477.

Sani H.A., Ahmad M.B., Hussein M.Z., Ibrahim N.A., Musa A. & Saleh T.A. (2017) Nanocomposite of ZnO with montmorillonite for removal of lead and copper ions from aqueous solutions. *Process Safety and Environmental Protection*, **109**, 97–105.

Sheydaei M. & Aber S. (2013) Preparation of nano-lepidocrocite and an investigation of its ability to remove a metal complex dye. *CLEAN – Soil, Air, Water*, **41**, 890–898.

Song M.-M., Branford-White C., Nie H.-L. & Zhu L.-M. (2011) Optimization of adsorption conditions of BSA on thermosensitive magnetic composite particles using response surface methodology. *Colloids and Surfaces B: Biointerfaces*, **84**, 477–483.

Sprynskyy M., Buszewski B., Terzyk A.P. & Namiesnik J. (2006) Study of the selection mechanism of heavy metal (Pb^{2+}, Cu^{2+}, Ni^{2+}, and Cd^{2+}) adsorption on clinoptilolite. *Journal of Colloid and Interface Science*, **304**, 21–28.

Stojakovic D., Milenkovic J., Daneu N. & Rajic N. (2011) A study of the removal of copper ions from aqueous solution using clinoptilolite from Serbia. *Clays and Clay Minerals*, **59**, 277–285.

Sun W., Meng Q., Jing L., He L. & Fu X. (2014) Synthesis of long-lived photo-generated charge carriers of Si-modified α-Fe$_2$O$_3$ and its enhanced visible photocatalytic activity. *Materials Research Bulletin*, **49**, 331–337.

Wang H.Y. & Huang H.F. (2010) Competitive adsorption of lead, copper and zinc ions on polymeric Al/Fe modified clinoptilolite. *Advanced Materials Research*, **156–157**, 900–907.

Wang M., Liao L., Zhang X., Li Z., Xia Z. & Cao W. (2011) Adsorption of low-concentration ammonium onto vermiculite from Hebei Province, China. *Clays and Clay Minerals*, **59**, 459–465.

Wang Z., Ma Y., He H., Pei C. & He P. (2015) A novel reusable nanocomposite: FeOOH/CBC and its adsorptive property for methyl orange. *Applied Surface Science*, **332**, 456–462.

Wu J., Zhang H., Oturan N., Wang Y., Chen L. & Oturan M.A. (2012) Application of response surface methodology to the removal of the antibiotic tetracycline by electrochemical process using carbon-felt cathode and DSA (Ti/RuO$_2$–IrO$_2$) anode. *Chemosphere*, **87**, 614–620.

Xu L., Cui H., Zheng X., Liang J., Xing X., Yao L., Chen Z. & Zhou J. (2018) Adsorption of Cu^{2+} to biomass ash and its modified product. *Water Science and Technology*, **2017**, 115–125.

Zhang G., Gao Y., Zhang Y. & Guo Y. (2010) Fe$_2$O$_3$-pillared rectorite as an efficient and stable Fenton-like heterogeneous catalyst for photodegradation of organic contaminants. *Environmental Science & Technology*, **44**, 6384–6389.